Chapter 5
Capturing 3D Mode Shapes with Cell Phone Videos

Shawn Richardson and Mark Richardson

Abstract Everyone has a cell phone in their pocket which has a video camera in it. A cell phone video is a low-cost, non-contacting way of recording the vibration of rotating machinery and the resonant vibration of mechanical structures. A cell phone can be used as a quick way to visualize vibration and complement other **ODS** and **Modal** testing methods

For this paper, **ODS-FRF** measurement functions were calculated from time waveforms (**TWFs**) that were extracted from cell phone videos of a rotating machine. Then the **ODS-FRFs** were curve fit using **FRF-based** curve fitting to yield **2D OMA** mode shapes of the machine. Two sets of **2D OMA** mode shapes were extracted from videos recorded at ***right angle views*** of the machine, one from the **Side** and one from the **Top**.

Then, **3D OMA** mode shapes were created by adding the mode shape components from the missing third direction to the **2D OMA** mode shapes from each view. The only requirement for preserving the phases of the missing mode shape components is that the **ODS-FRFs** share a common reference response.

Keywords Time Waveform (**TWF**) · Digital Fourier Transform (**DFT**), Auto Power Spectrum (**APS**) · Cross Power Spectrum (**XPS**).**ODS-FRF** · Operational Modal Analysis (**OMA**) mode shape

Rotating Machine

The test article used for this paper is shown on Figure 1. The machine speed was fixed at ***approximately* 1000 RPM** throughout all the cell phone video recordings.

For this paper, all cell phone videos were recorded with one screw added to both the inner and outer rotor. Previous papers [1, 2] have presented results when different unbalancing screws were used to a similar rotating machine.

Introduction

Using accelerometers for data acquisition is more expensive and time-consuming to implement when compared to recording a cell phone video. Furthermore, because it is non-contacting, a cell phone can record vibration of machinery or structural parts that are too hot, too dangerous, or are inaccessible for attaching accelerometers.

TWFs & DFTs

In previous papers [1] to [4], traditional signal processing methods were applied to the **TWFs** extracted from the frames of a video. **TWFs** can be used to display **time-based ODSs** on a point grid, allowing vibration to be visualized at slower speeds with higher amplitudes. And their associated **DFTs** can be used to display **frequency-based ODS**'s using sinusoidal animation of the **ODS** at the cursor location in the **DFTs**.

When a video is processed in MEscope [10], a rectangular grid of points with surfaces between them is created. Video frames are attached to this surface during animated display of Video ODS's. Using a point grid, millions of pixels per frame

Shawn Richardson and Mark Richardson
Vibrant Technology, Inc., Centennial, CO
e-mail: shawn.richardson@vibetech.com; mark.richardson@vibetech.com

© The Author(s), under exclusive license to River Publishers 2026

Kristin B. Zimmerman, PhD (eds.), *Computer Vision and SLDV for Structural Dynamics, 2026, Vol. 6*, Conference Proceedings of the Society for Experimental Mechanics Series, https://doi.org/10.13052/rp-9788743814177

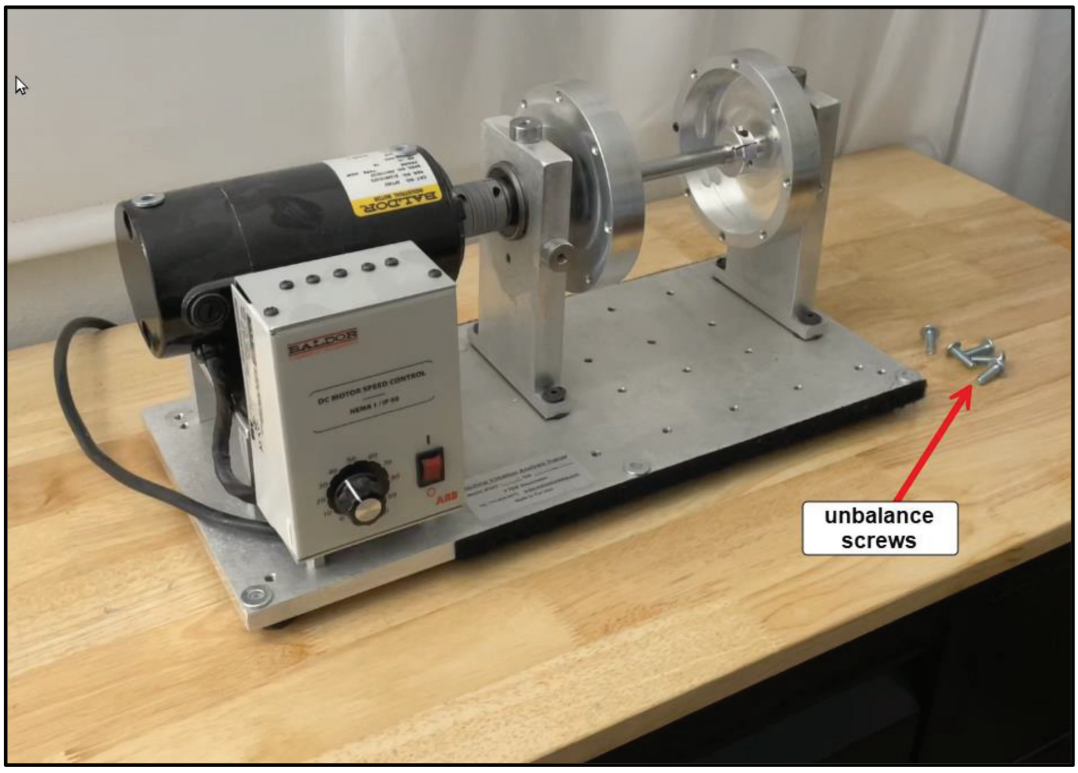


Fig. 1 Rotating Machine Showing Unbalance Screws Added to Its Rotors

of a cell phone video are processed to extract TWFs for the horizontal & vertical deflections of thousands of points in the point grid. Grid points with little or no motion, (e.g. background points), are hidden and their linked TWFs removed from further analysis.

A DFT is calculated from each TWF that is extracted from the video. Time-based ODS's are displayed in animation from the TWFs using a sweeping Line cursor. Frequency-based ODS's are displayed in animation from the DFTs using sinusoidal dwell modulation of the ODS at a cursor position. The magnitude & phase of the ODS at selected grid points can also be displayed, as shown in Figures 2 & 3.

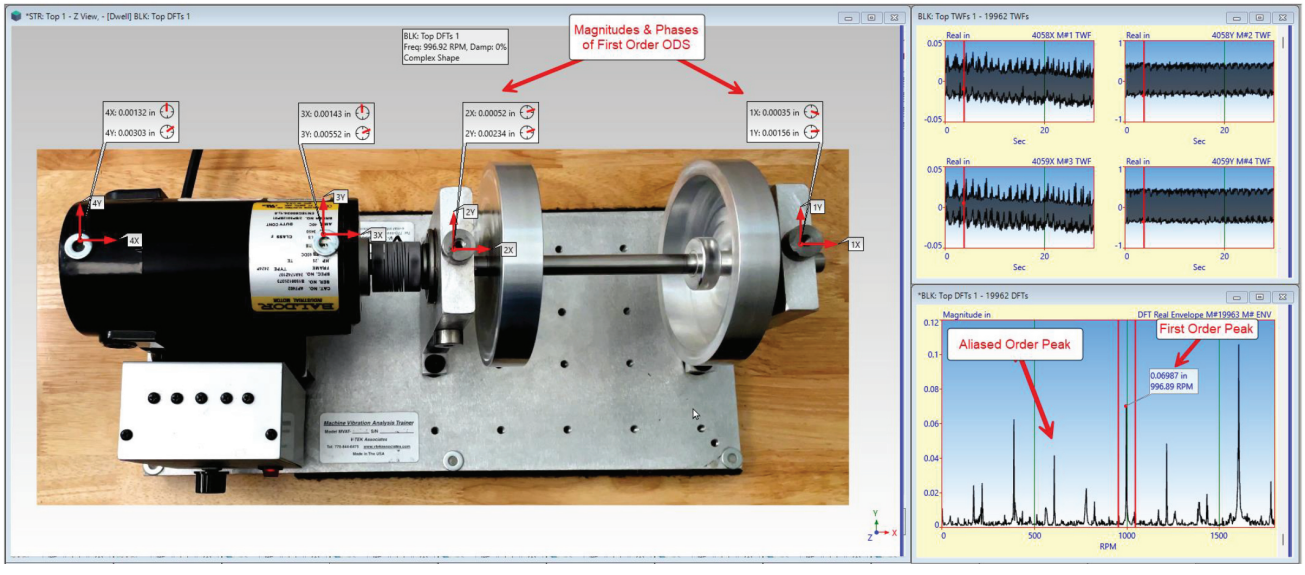


Fig. 2 Top View-First-Order ODS Animated from DFTs

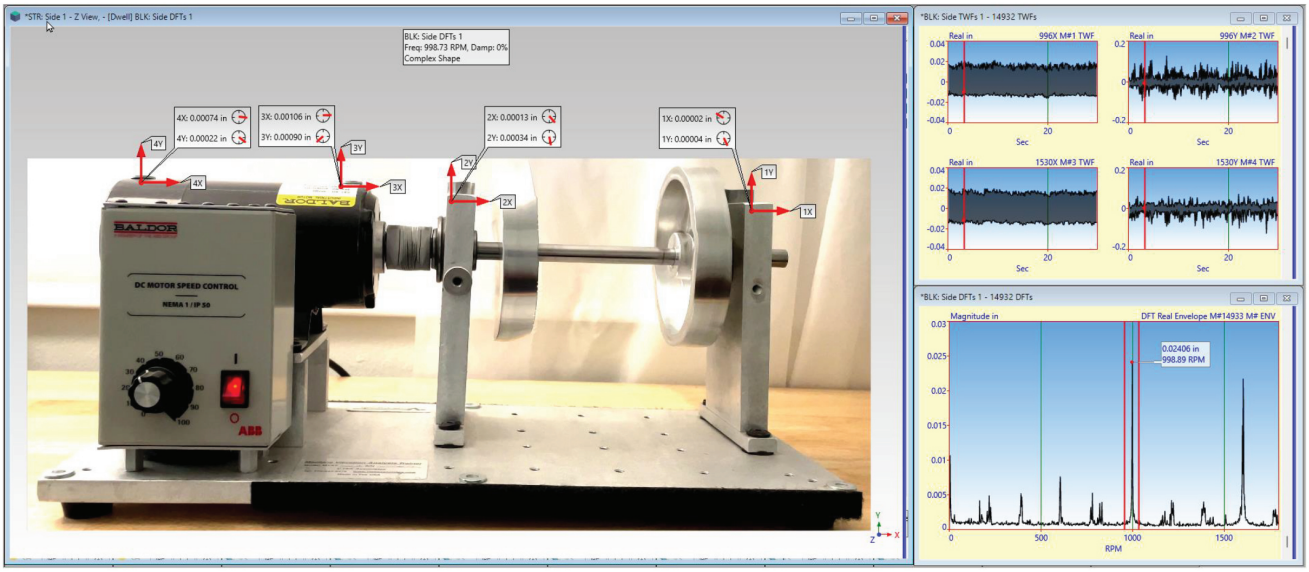


Fig. 3 Side View-First-Order ODS Animated from DFTs

ODS-FRFs

A unique frequency domain function, called an **ODS-FRF,** can be calculated from each response **TWF** extracted from a video. A set of **ODS-FRFs** calculated from the **TWFs** is typically more accurate than **DFTs** because ***spectrum averaging*** can be used to reduce extraneous noise from the **ODS-FRFs**, and **Hanning** windowing can be used to ***reduce signal leakage*** from the resonance peaks.

The ***magnitude*** of an **ODS-FRF** is the **APS** of a ***response*** **DOF** at a grid point. The ***phase*** of the **ODS-FRF** is the ***phase of the*** **XPS** between the ***response*** **DOF** and the **DOF** of any ***reference*** grid point.

ODS-FRFs carry the ***same units*** as the response **TWFs** from which they are calculated. Unlike an **XPS**, an **ODS-FRF** in displacement units can be ***accurately differentiated to velocity units*** by multiplying it by the frequency variable.

Vibration in ***velocity units*** is commonly used by vibration analysts to quantify vibration levels in rotating equipment.

One of the laws of the **FFT** algorithm is that $\mathbf{\Delta f = 1/T}$, where $\mathbf{\Delta f}$ is the ***frequency difference between samples*** of an **ODS-FRF**, and **T** is the ***time length*** of **TWF** data from which the **ODS-FRF** was calculated. For example, if an **ODS-FRF** is calculated from a **TWF** using **25 second**s of uniformly sampled data, the frequency resolution ($\mathbf{\Delta f}$) of the **ODS-FRF** is **60/25 = 2.4 RPM**.

To increase the frequency resolution of an **ODS-FRF**, **TWF** data over a ***longer period*** **T** is required. Therefore, the video from which the **TWFs** are extracted must be recorded over a ***longer period*** **T**.

Aliased Order Peaks

A limitation of any video recording is that ***anti-alias filtering cannot be used*** to remove high-frequency signals from the video.

Without anti-alias filtering, machine order peaks ***at frequencies greater than one-half the sampling frequency***, (called **Fmax)**, are ***folded around*** **Fmax** and appear at lower frequencies in the **ODS-FRFs**, as shown in Figures 2, 3, & 4.

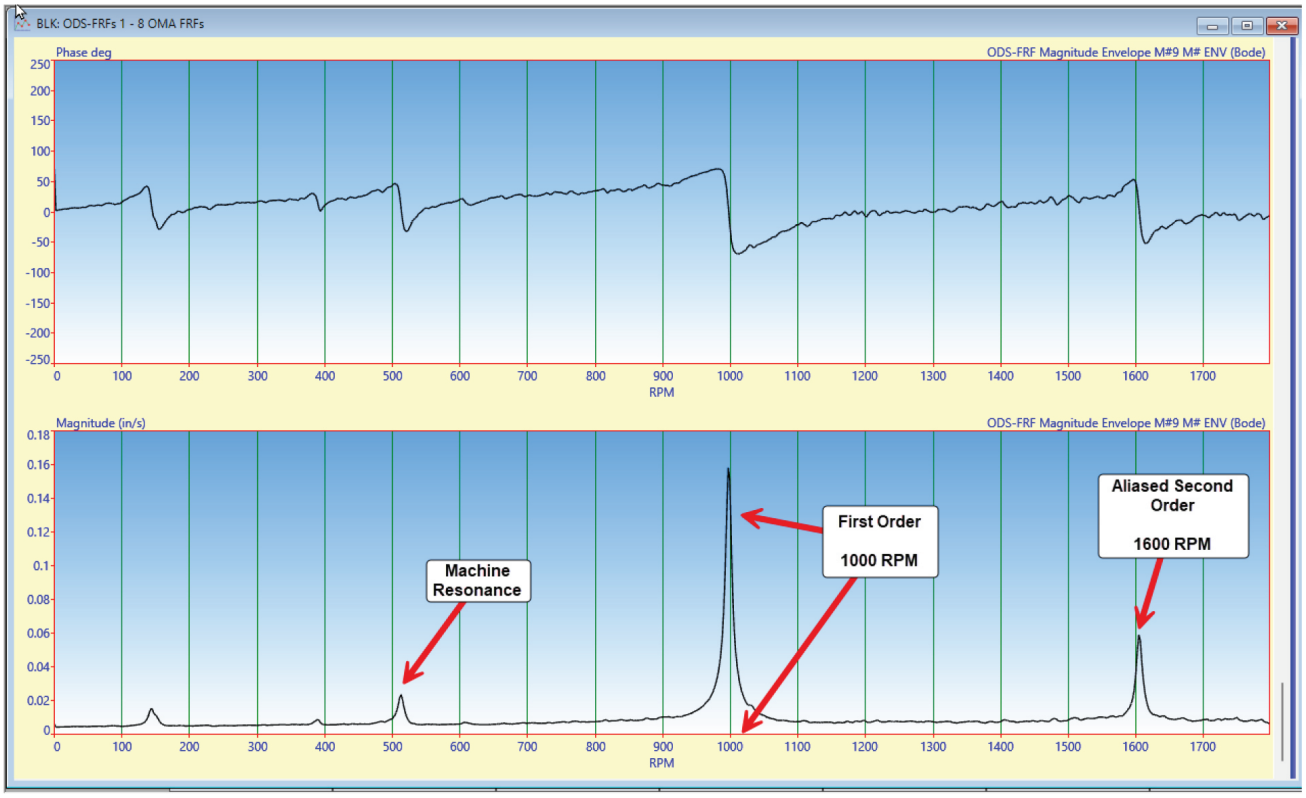


Fig. 4 ODS-FRF Showing First Order, Aliased Second & Machine Resonance

All machine-order resonance peaks between **Fmax & 2x Fmax** are folded around (***wrapped around***) **Fmax** and appear at lower frequencies in the frequency band **(0 to Fmax)**. Aliasing of higher frequencies occurs in both **DFTs** and **ODS-FRFs**.

The magnitude of the **ODS-FRF** shown in Figure 4 was calculated from a **TWF** that was extracted from a video that was sampled at **60 fps**, or **3600 RPM**. Therefore, the **Fmax** of the **ODS-FRF** is **1800 RPM**. The first-order peak is at the machine running speed and is clearly visible at **approximately 1000 RPM**. The second order resonance peak should be at about **2000 RPM** and third order resonance peak should be at about **3000 RPM, etc.** Aliased order peaks are clearly visible ***at lower frequencies*** in the **DFTs** and the **ODS-FRFs**.

The **ODS** or **OMA** mode shape of an aliased order is correct. Only its frequency is incorrect.

The aliased frequency of an order higher than **Fmax** can be calculated from **Fmax** and the expected order frequency.

- **Second order** aliased frequency → 1800 - (2000 - 1800) **1600 RPM**
- **Third order** aliased frequency → 1800 - (3000 - 1800) **600 RPM**
- **Fourth order** aliased frequency → 1800 –((3600 - (4000 - 3600)) -1800) **400 RPM**

The **ODS-FRF** in Figure 4 was calculated from a **TWF** with ***a 25-second length***. Therefore, **Δf = (1/25) Hz or 60/25 = 2.4 RPM** and the aliased frequency of the third order peak is ***within one*** **(Δf)** of its calculated value.

Curve Fitting the ODS-FRFS

ODS-FRFs can be curve-fit using an **FRF-based** curve fitter if they have been filtered with a special window. In MEscope [10] this filter is called a ***DeConvolution window***. This filter reshapes an **ODS-FRF** so that it resembles an **FRF** waveform and therefore can be curve fit using **FRF-based** curve fitting. An **FRF-based** curve fit of an **ODS-FRF** is shown in Figure 5. In the upper left-hand graph, the **red curve fitting function** is overlaid on a magnitude plot of the **ODS-FRF**.

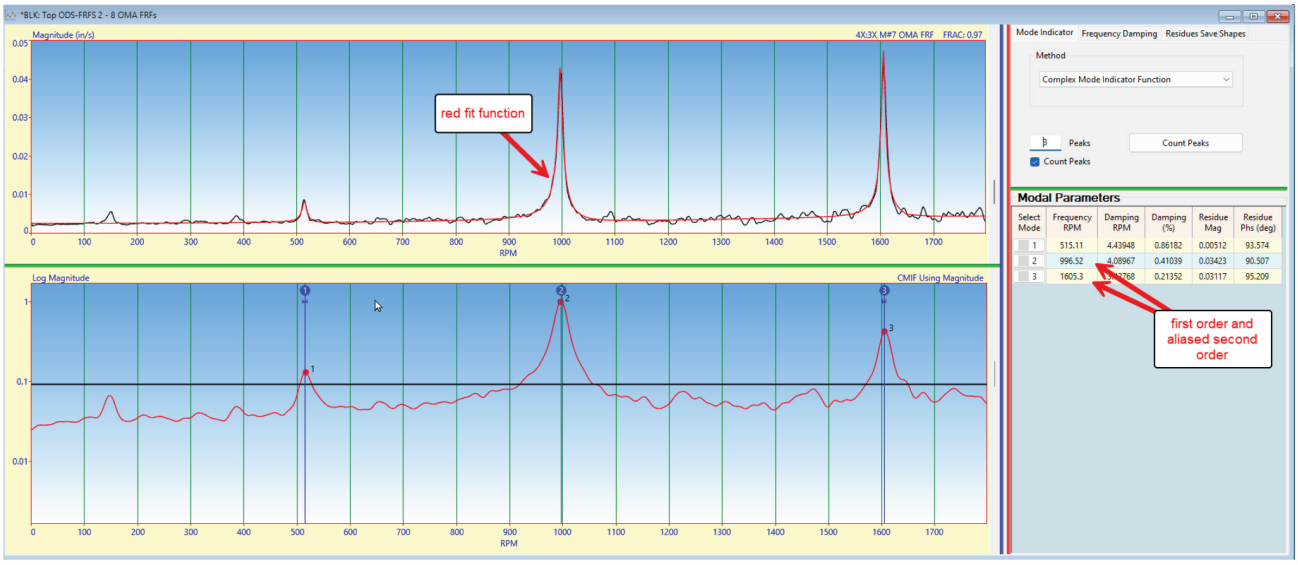


Fig. 5 Curve Fit of ODS-FRFs.

Comparing Mode Shapes from Successive Side View Videos

Two successive video recordings from a **Top** view of the rotating machine were post-processed and the resulting mode shapes were compared using two different shape correlation coefficients, the Modal Assurance Criterion (**MAC**) and the Shape Difference Indicator (**SDI**). Both correlation coefficients have values between 0 and 1. A value of **"0"** means that two shapes are different from one another, and a value of **"1"** means that two mode shapes are the same.

Each shape has 8 components corresponding to X & Y deflections at 4 grid points. Two points are on the motor, and one is on the top of each bearing block. The **MAC** & **SDI** values between the **OMA** mode shapes from two successive videos of the machine are shown on Figures 6 & 7.

In Figure 6, mode shapes 2 & 3 correlate well from two successive **Side** view videos, with **MAC** & **SDI** values above 90% In Figure 7, all three mode shapes correlate well from two successive **Top** view videos, with **MAC** & **SDI** values above 90%.

The low values of the off-diagonal MAC & SDI values indicate that the three **OMA** mode shapes have different magnitudes & phases. This becomes clear when the magnitudes & phases of the mode shapes are displayed on the point grid.

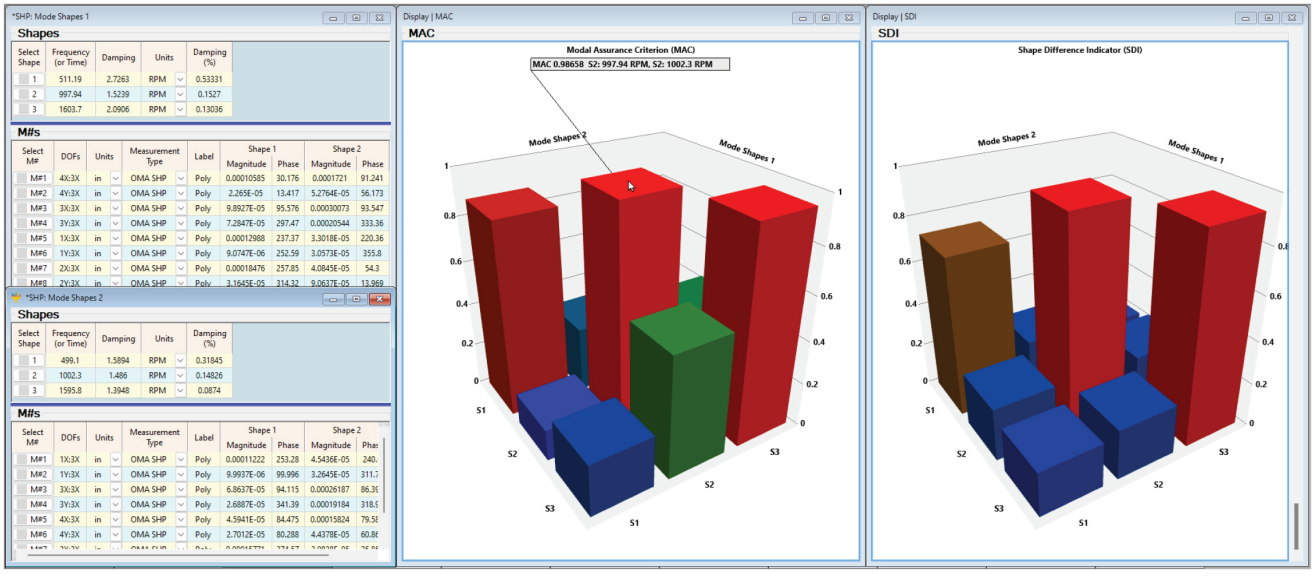


Fig. 6 MAC & SDI of Mode Shapes From Two Sucessive Side Videos

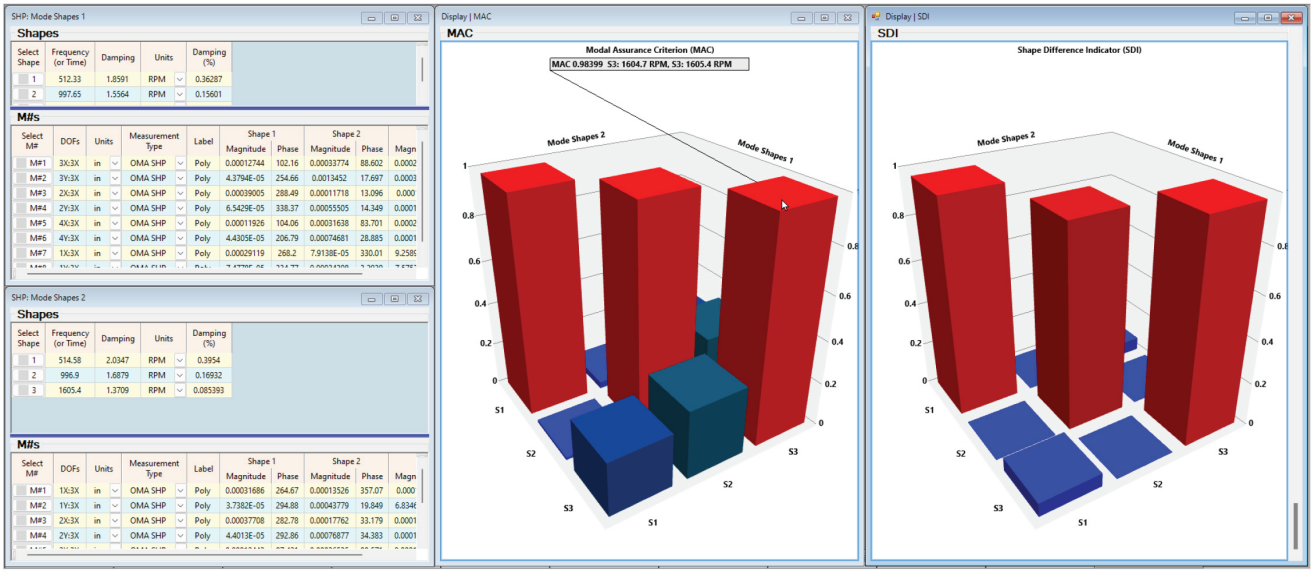


Fig. 7 MAC & SDI of Mode Shapes From Two Sucessive Top Videos

Comparing Mode Shapes from Successive Top View Videos

Two successive video recordings from a side view of the rotating machine were post-processed and the resulting mode shapes are compared the Modal Assurance Criterion (MAC) and the Shape Difference Indicator (SDI) in Figure 6.

Side View Animated Display of the 3D OMA Mode Shapes

Animation of the **3D OMA** mode shape of the first order at **997 RPM** from the **Side** view is shown in Figure 8. In the X-direction the motor and inner bearing block are in-phase, and the outer bearing block is 180 degrees out-of-phase. In the Y-direction, the front side of the motor is in-phase with both bearing blocks and the back side is 90 degrees out-of-phase. In the Z-direction, the motor and bearing blocks are all in-phase with one another.

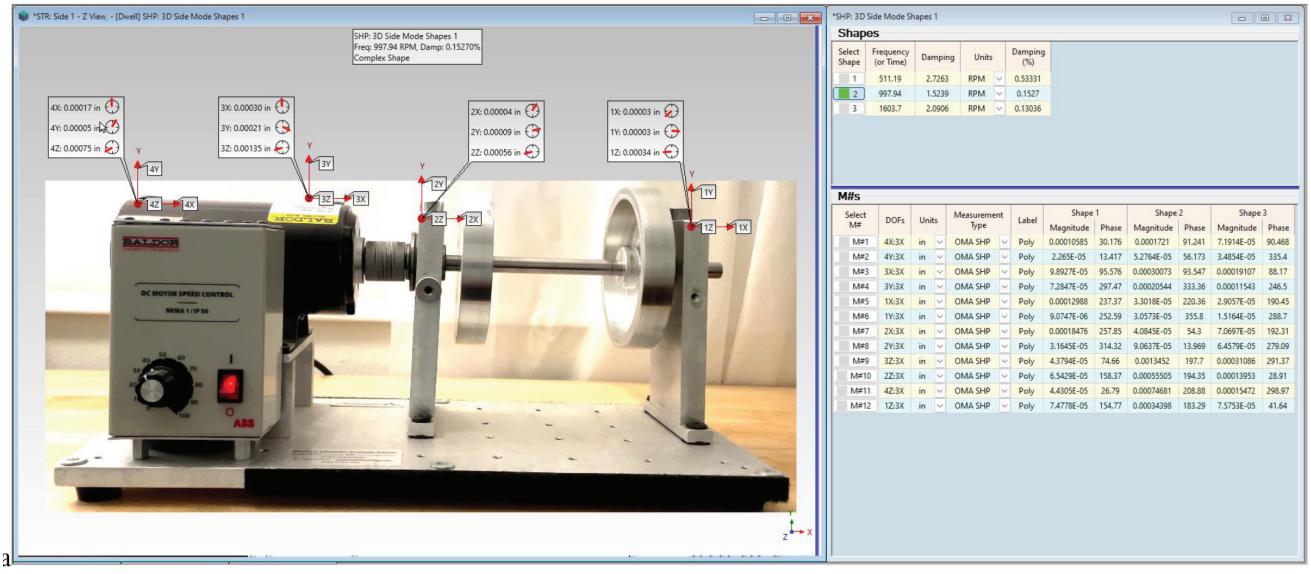


Fig. 8 Side View - Animated Deflection of the First-Order OMA Mode Shape

Top View Animated Display of the 3D OMA Mode Shapes

Animation of the **3D OMA** mode shape of the first order at **997 RPM** is shown in Figure 9. In the X-direction the motor is 90 degrees out-of-phase with the bearing blocks. In the Y-direction, the motor and bearing blocks are in-phase. This agrees with the Z-direction in the Side view. In the Z-direction, the front side of the motor is in-phase with both bearing blocks and the back side is out-of-phase. This agrees with the Y-direction in the Side view.

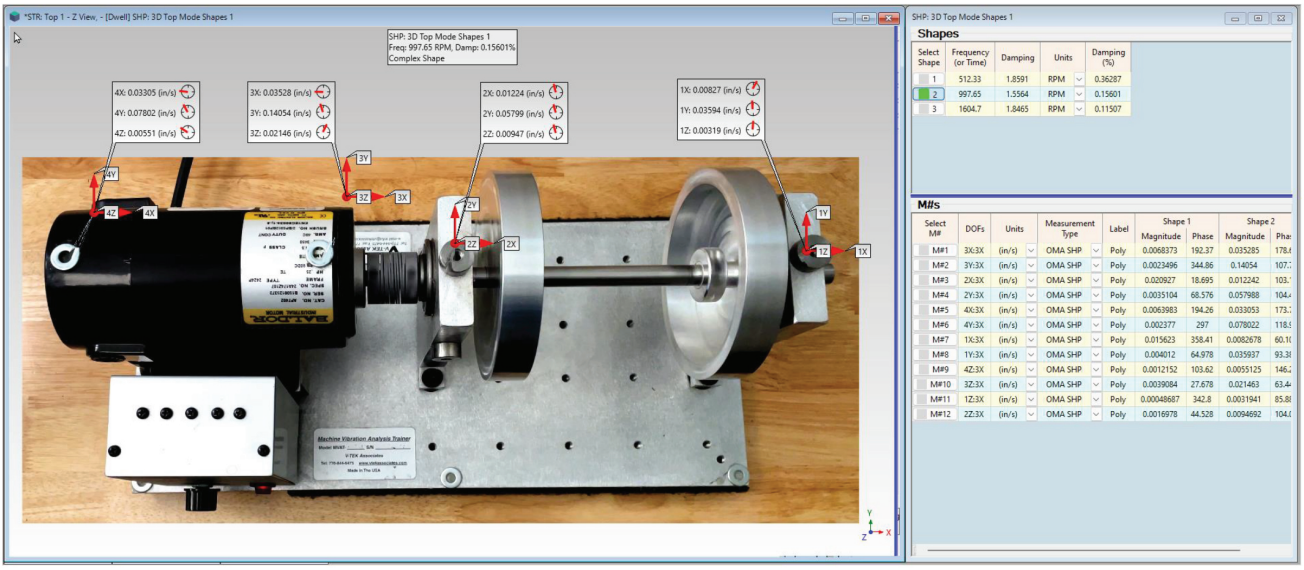


Fig. 9 Top View - Animated Deflection of the First-Order OMA Mode Shape

Conclusions

In this paper, we extracted **2D** mode shapes from two successive videos of the **Top** view and **Side** view of a rotating machine while it was running at approximately **1000 RPM**. Then, **ODS-FRFs** were calculated from the **TWFs** using **25-seconds** of data per average, 5 spectrum averages with 95% overlap processing and a Hanning window to reduce signal leakage from the resonance peaks. Then the **ODS-FRFs** were windowed with a Deconvolution window to prepare them for **FRF-based** curve fitting. **2D OMA** mode shapes of a rotating machine were obtained by applying **FRF-based** curve fitting to the **ODS-FRFs**.

The **ODS-FRFs** contained three peaks, the running speed at **1000 RPM**, the aliased second order at **1800 RPM**, and a machine resonance at **500 RPM**.

The **2D OMA** mode shapes obtained from curve fitting **ODS-FRFs** calculated from successive videos of the Top and Side of the machine were correlated using the Modal Assurance Criterion (**MAC**) and Shape Difference Indicator (**SDI**). Mode shape pairs with coefficients above 90% correlated well.

Finally, **3D OMA** mode shapes of the machine were created by adding the Y-direction mode shape components from the **Top** view as Z-direction components to the mode shapes of the **Side** view. Likewise, the Y-direction mode shape components from the **Side** view were added as Z-direction components to the mode shapes of the **Top** view.

All mode shape phases were preserved by using **DOF 3X** as the reference for the **ODS-FRF** calculations. No tachometer signal of other means of matching phases is needed when **ODS-FRFs** are calculated using the same reference response **DOF**.

References

1. S. Richardson, M. Richardson “Using Mode Shapes From Cell Phone Videos For Machinery Health Monitoring” VIATC 2025 Newport News, VA August 6-8, 2025
2. S. Richardson, M. Richardson “Extracting 3D Mode Shapes from a Cell Phone Video” IMAC XLII Orlando, FL February 10-13, 2025

3. D. Ambre, B. Schwarz, S. Richardson, M. Richardson, “Using Cell Phone Videos to Diagnose Machinery Faults” IMAC XLI Austin, TX February 13-16 2023
4. B. Schwarz, S. Richardson, M. Richardson, “Using a Cell Phone Video and ODS Correlation to Diagnose Unbalance in Rotating Machinery” IMAC XLII January 29 - February 1, 2024 Orlando, FL
5. M.H. Richardson, “Is It a Mode Shape or an Operating Deflection Shape?” Sound and Vibration magazine March 1997
6. B. Schwarz, M.H. Richardson, “Measurements Required for Displaying Operating Deflection Shapes” Proceedings of IMAC XXII January 26, 2004
7. B. Schwarz, M.H. Richardson, “Introduction to Operating Deflection Shapes” CSI Reliability Week Orlando, FL October 1999
8. S. Richardson, J. Tyler, P. McHargue, M. Richardson “A New Measure of Shape Difference” IMAC XXXII February 3-6, 2014
9. S. Richardson, J. Tyler, B. Schwarz, P. McHargue, M. Richardson “Using Modal Parameters for Structural Health Monitoring” IMAC-XXXV Garden Grove, CA January 30–February 2, 2017
10. MEscope$^{\mathrm{TM}}$ is a trademark of Vibrant Technology, Inc. www.vibetech.com